



# Ferumoxytol-enhanced vascular suppression in magnetic resonance neurography

Sophie C. Queler<sup>1</sup> · Ek Tsoon Tan<sup>1</sup> · Christian Geannette<sup>1</sup> · Martin Prince<sup>2</sup> · Darryl B. Sneag<sup>1</sup>

Received: 21 March 2021 / Revised: 27 April 2021 / Accepted: 27 April 2021 / Published online: 7 May 2021  
© ISS 2021

## Abstract

**Objective** To evaluate ferumoxytol-enhanced vascular suppression for visualizing branch nerves of the brachial plexus in magnetic resonance (MR) neurography.

**Materials and methods** Signal simulations were performed to determine ferumoxytol's effect on nerve-, fat-, and blood-to-muscle contrast and to optimize pulse sequence parameters. Prospective, in vivo assessment included 10 subjects with chronic anemia who underwent a total of 19 (9 bilateral) pre- and post-infusion brachial plexus exams using three-dimensional (3D), T<sub>2</sub>-weighted short-tau inversion recovery (T<sub>2</sub>-STIR) sequences at 3.0 T. Two musculoskeletal radiologists qualitatively rated sequences for the degree of vascular suppression and brachial plexus branch nerve conspicuity. Nerve-to-muscle, -fat, and -vessel contrast ratios were measured.

**Results** Quantitative nerve/muscle and nerve/small vessel contrast ratios (CRs) increased with ferumoxytol ( $p < 0.05$ ). Qualitative vascular suppression and suprascapular nerve visualization improved following ferumoxytol administration for both raters ( $p < .05$ ). Pre- and post-ferumoxytol exams demonstrated moderate to near-perfect inter-rater agreement for nerve visualization and diagnostic confidence for the suprascapular and axillary nerves but poor to no agreement for the long thoracic nerve.

**Conclusion** Ferumoxytol in T<sub>2</sub>-weighted brachial plexus MR neurography provides robust vascular suppression and aids visualization of the suprascapular nerve in volunteers without neuropathy.

**Keywords** MRI · Brachial plexus · MR neurography · Ferumoxytol · Peripheral nerve · Muscle

## Introduction

Magnetic resonance (MR) neurography relies on heavily T<sub>2</sub>-weighted sequences for reliable identification and evaluation of peripheral nerves [1]. Nerves have similar relaxivity values and morphology to blood vessels, however, making it challenging to distinguish them from adjacent vasculature [2]. Non-contrast techniques for vascular suppression depend on blood motion for dephasing vascular signal [3–5]; these techniques are effective in suppressing fast-flowing blood but less effective for slow-flowing blood in the small

veins that often accompany peripheral nerves [6–9]. Venous contamination makes small nerves challenging to visualize, even when pathologic and enlarged [10].

Intravenous gadolinium shortens both the longitudinal (T<sub>1</sub>) and transverse (T<sub>2</sub>) relaxation times of the blood [11]. Gadolinium-based contrast agents can consequently be used for vascular suppression in MR neurography in combination with velocity-based methods [12–14]. However, rapid redistribution of gadolinium into the extracellular compartment and concern over nephrogenic systemic fibrosis and tissue gadolinium deposition, particularly in individuals with chronic kidney disease or who require repeat contrast administration, warrants investigation into alternative contrast agents [15–19].

Ferumoxytol is an ultrasmall, superparamagnetic iron oxide nanoparticle with a semi-synthetic carbohydrate shell. This coating isolates the bioactive iron from serum components until the molecule can be phagocytosed by Kupffer cells, thereby increasing its half-life and reducing its immunogenicity [20]. Though originally developed as a

✉ Darryl B. Sneag  
sneagd@hss.edu

<sup>1</sup> Department of Radiology and Imaging, Hospital for Special Surgery, New York, NY, USA

<sup>2</sup> Department of Radiology, New York-Presbyterian/Weill Cornell Medical Center, 535 E. 70th St., New York, NY 10021, USA

blood-pool contrast agent in injectable bolus form, ferumoxytol received FDA approval in 2009 to treat iron deficiency anemia (IDA) in adults with chronic kidney disease. Today, ferumoxytol remains a common treatment for IDA but continues to garner interest over its many “off-label” diagnostic and “theranostic” imaging applications [11, 21–25].

Ferumoxytol’s long intravascular half-life of 10–15 h, compared to 1.5 h for most gadolinium-based agents, makes it amenable to longer MRI scans and confers greater flexibility in timing between administration and MR acquisition. Furthermore, ferumoxytol remains intravascular, which is an advantage for venous suppression compared to agents like gadolinium that rapidly redistribute into other compartments. Like gadolinium, ferumoxytol causes both  $T_1$  and  $T_2$  shortening but has much stronger  $T_2^*$  (and  $T_2$ ) effects [22, 26]. This suggests that ferumoxytol could be more effective when used for vascular suppression than for vascular enhancement. Ferumoxytol has been shown to achieve effective vascular suppression for slow-flowing veins in MR lymphangiography [27, 28] but to our knowledge has not been used for  $T_2$ -weighted fast spin echo (FSE) in MR neurography.

The purpose of this study was to investigate the role of ferumoxytol for vascular suppression in MR neurography of the brachial plexus. We hypothesized that ferumoxytol would improve quantitative nerve/muscle and nerve/vessel contrast ratios (CRs), as well as qualitative vascular signal suppression, nerve visualization, and diagnostic confidence compared to a non-contrast technique.

## Materials and methods

This study was approved by our Institutional Review Board (IRB) and was compliant with the Health Insurance Portability and Accountability Act. Written informed consent

was obtained from all individual participants included in the study.

## Signal simulations

Signal simulations were first performed to determine (i) the effects of ferumoxytol infusion on nerve-, fat-, and blood-to-muscle contrast and (ii) the optimal pulse sequence parameters for imaging. We aimed to optimize nerve signal while maximizing nerve-to-fat, nerve-to-muscle, and nerve-to-blood CRs. Bloch equations were used to determine the signals obtained during FSE readout. Model parameters are listed in Table 1, including  $T_1$  and  $T_2$  relaxation times for nerve, blood, fat, and muscle, as well as relaxation rates for ferumoxytol and gadolinium [22]. The vessel signals were computed with and without infusion, assuming a steady-state concentration between 5 and 100% of a single dose (510 mg iron) of ferumoxytol in a standard-size patient (83 kg). A gadolinium-based contrast agent, gadobutrol (Gadovist™, 0.1 mL/kg) was also simulated for comparison. A signal-to-noise ratio of 200 was assumed in the calculation of tissue CRs.

We evaluated inversion times (TI) ranging from 100 to 260 ms, with the latter being just past the null point for fat at 3.0 T (T) (approximately 250–255 ms). The echo times (TE) evaluated ranged from 30 to 120 ms. To simulate the effects of non-contrast vascular suppression using crusher gradients, the velocity of the blood was varied between 3 and 6 cm/s along the direction of the crusher gradient, which was at a strength of 2.5 (relative to slab-encoding). The velocity of the fluid in the nerves was assumed to be negligible (under 3 mm/s). Unless otherwise stated, the simulated timing parameters were as follows: repetition time (TR) = 3500, TE = 80, TI = 250, echo spacing = 5 ms.

**Table 1** MRI relaxation times for different tissue types at 3.0 T and relevant concentration relaxation rates and assumptions for ferumoxytol

Tissue type	Longitudinal relaxation time, $T_1$ (msec)	Transverse relaxation time, $T_2$ (msec)
Tissue relaxation times		
Blood	2000	250
Nerve	1400	150
Fat	371	173
Muscle	1500	35
Contrast agent simulation parameters		
Parameter	Ferumoxytol	Gadovist
Longitudinal relation rate, $r_1$ ( $\text{mM}^{-1} \text{s}^{-1}$ )	9.46	5.0
Transverse relaxation rate, $r_2$ ( $\text{mM}^{-1} \text{s}^{-1}$ )	65.2	7.1
Dose	510 mg Fe	0.1 mL/kg, 0.1 mmol/kg
Average mass of subject (kg)	83.2	
Average blood volume (L)	5.62	

## Human subjects

To prospectively evaluate the efficacy of ferumoxytol-enhanced vascular suppression *in vivo*, we consecutively enrolled adult patients with the diagnosis of chronic IDA who received ferumoxytol infusions at a nearby clinic between March and December 2019. Those with relative contraindications to MRI (e.g., implantable devices; claustrophobia; pregnancy), orthopedic hardware within the region of the brachial plexus, peripheral neuropathy, diabetes mellitus, or history of cervical or peripheral nerve surgery within the brachial plexus region were excluded. Subjects were additionally excluded if they had received a separate ferumoxytol infusion within the previous 4 weeks.

## Imaging protocol

A single recommended dose (510 mg elemental iron in 17 mL) of ferumoxytol (Feraheme, AMAG Pharmaceuticals, Inc, Waltham, MA, USA) diluted in 200 mL of normal saline was administered to each subject as a standard-of-care, slow infusion over 15 min (34 mg/min) for IDA. Dedicated brachial plexus MR neurography exams of right and/or left sides were acquired in each subject before and after infusion.

MR neurography exams were performed on a 3.0 T system (GE Healthcare, Waukesha, WI, USA) using a 32-channel (unilateral) or an IRB-approved, investigational 64-channel (bilateral) flexible, surface array, receive-only coil. The investigational coil enabled bilateral brachial plexus imaging without having to reposition the coil, thereby reducing overall scan time.

Pre- and post-infusion MR neurography involved three-dimensional (3D), T<sub>2</sub>-weighted short-tau inversion

recovery (T<sub>2</sub>-STIR) sequences of the targeted regions. Imaging parameters were as follows: field of view = 208, matrix (frequency × phase) = 208 × 208, slice thickness (no gap) = 1 mm, number of slices (median) = 112, TR/TE/TI = 3002/60–81/250 ms, receiver bandwidth = 195.31 Hz, number of excitations = 2, echo train length = 130. Crusher gradients were applied in the frequency (superior–inferior) and slice (anterior–posterior) directions for increased flow suppression, using default parameters provided by the MRI vendor. The study investigators monitored all exams in real time to ensure image quality and repeated sequences if necessary.

## Qualitative analysis

MR exams were anonymized and retrospectively interpreted by two radiologists (DBS, CG). Each rater had 7 years of musculoskeletal MRI experience; rater 1 (DBS) additionally had extensive, dedicated MR neurography experience within this time period. The radiologists were blinded to the sequence type and independently evaluated exams at random on a PACS workstation (Sectra IDS7, Linköping, Sweden) for (1) degree of vascular signal suppression; (2) ability to visualize the proximal and distal segments of the suprascapular, axillary, and long thoracic nerves (defined by uniform osseous landmarks, as described in Table 2); and (3) diagnostic confidence in evaluating each nerve segment. Diagnostic confidence was defined as “high” if the nerve segment could be identified on every image slice through which the nerve was expected to traverse and “low” if not visualized on all slices. The suprascapular, axillary, and long thoracic nerves were chosen for assessment as these nerves are commonly evaluated in clinical practice and can be difficult to assess on routine MR neurography exams due to

**Table 2** Three-point qualitative scoring system utilized for assessing vascular suppression, nerve visualization, and diagnostic confidence of each nerve segment

Score	Vascular suppression	Nerve visualization <sup>*†</sup>	Diagnostic confidence <sup>**‡</sup>
0	-	No visualization	Low confidence
1	Arterial only	Partial visualization	High confidence
2	Arterial and partial venous	Full visualization	-
3	Complete arterial and venous	-	-
Nerve	Osseous landmark	Proximal segment	Distal segment
Suprascapular	Clavicle	Supra-/retroclavicular	Infraclavicular
Axillary	Inferior glenoid	Posterior cord to the inferior glenoid	Inferior glenoid to quadrilateral space
Long thoracic	Clavicle	Supraclavicular	Infraclavicular

\*Proximal and distal segments of the suprascapular, axillary, and long thoracic nerves were individually evaluated

†Complete nerve visualization (the highest qualitative score) was defined as the identification of the nerve on every image slice through which the nerve was supposed to course

‡Complete diagnostic confidence was defined as a reliable evaluation of the entire nerve segment towards making a diagnosis

inadequate vascular suppression. Qualitative evaluation was based on a 3-point scale, as outlined in Table 2.

## Quantitative analysis

Nerve conspicuity was quantitatively assessed relative to muscle, fat, and vessel. Mean nerve-to-muscle, nerve-to-fat, nerve-to-large-vessel, and nerve-to-small-vessel CRs were calculated using manually drawn regions of interest within the C6 nerve root, anterior scalene muscle, subcutaneous fat, subclavian artery (large vessel), and suprascapular artery (small vessel) (Fig. 1).

## Statistical methods

This study was powered a priori to detect a difference in CR between pre- and post-ferumoxytol exams based on results from a previous study [14]. A sample size of 10 paired (pre- and post-ferumoxytol) exams would achieve 80% power to detect a difference of 0.8 between contrast and non-contrast CRs with a 0.7 standard deviation and an alpha level of 0.05 using a paired *t*-test.

Change in vascular suppression, nerve conspicuity, and diagnostic confidence scores was calculated as median differences with interquartile ranges (IQR) by rater and nerve segment. Scores were compared using the paired cluster-weighted signed rank test [29–31]. Inter-rater agreement was evaluated using Gwet's chance-adjusted agreement coefficient (AC). Gwet's AC has the advantage of not relying on independence between measurements, making it suitable for the dependent measurements due to bilaterality [32]. CRs of pre- and post-ferumoxytol imaging were compared using a linear regression model with random subject effects

to account for those with bilateral imaging. Mean CR differences with 95% confidence intervals (CI) are reported. Statistical significance was set a priori to  $p < 0.05$ . Statistical analyses were performed with SAS version 9.4 (SAS Institute, Cary, NC, USA) and R version 4.0.3 using the *hstestClust* package [33].

## Results

### Signal simulations

Figure 2 shows the (a) STIR-FSE pulse sequence diagram and the resulting (b) longitudinal magnetization and (c) signal magnitudes for various tissues. The simulated signal levels were taken at the chosen echo time, which was nominally the 16th echo (five FSE echoes prior to the first echo were discarded to achieve a steady state). There was a greater signal reduction in ferumoxytol + blood relative to both gadolinium + blood and blood without contrast agent.

Simulations demonstrated that despite decreased nerve signal with increasing TI (Fig. 3a), an optimum TI = 250–255 ms was desirable to achieve high nerve/fat CR (Fig. 3b), especially since other nerve/tissue CRs were fairly constant with changes in TI. Simulations also showed that since nerve/(ferumoxytol + blood) CR was fairly constant with TE (Fig. 3d), it was desirable to keep an intermediate TE of 60–80 ms to balance nerve signal decrease (Fig. 3c) versus nerve/muscle CR increase with TE (Fig. 3d).

While vascular signal suppression was less effective at low velocities, simulations showed that administration of either gadolinium (Fig. 4a) or ferumoxytol (Fig. 4b)

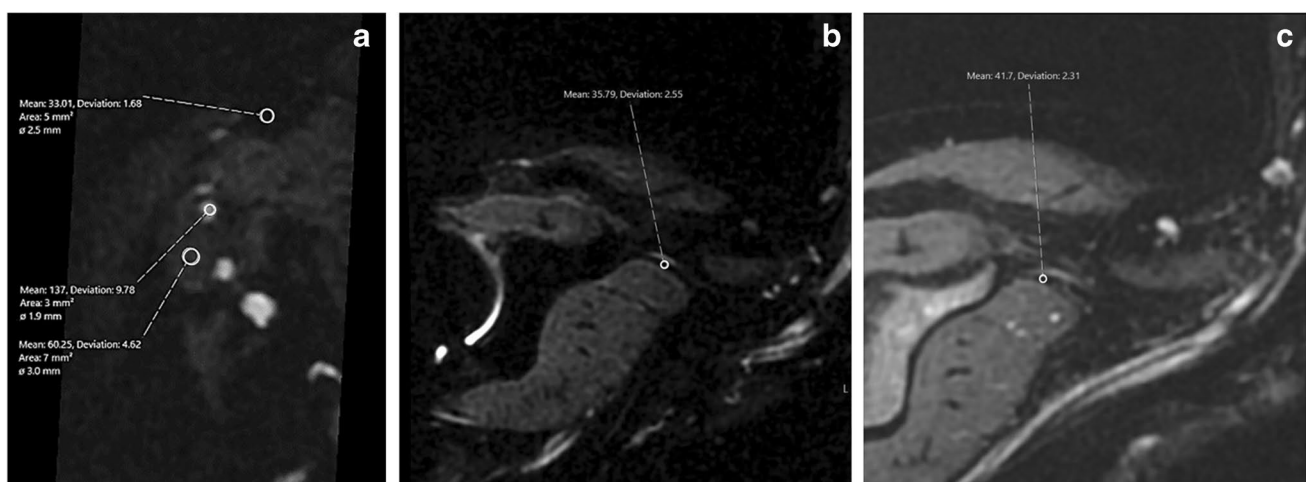


**Fig. 1** Example of regions of interest (ROIs) placed on the subcutaneous fat (top ROI), the C6 nerve root (in cross-section) (middle ROI), and within the anterior scalene muscle (bottom ROI) on the post-fer-

umoxytol MRI (a). Pre- (b) and post- (c) ferumoxytol exams in the same volunteer demonstrate ROI placement within the suprascapular artery, inferior to the suprascapular nerve

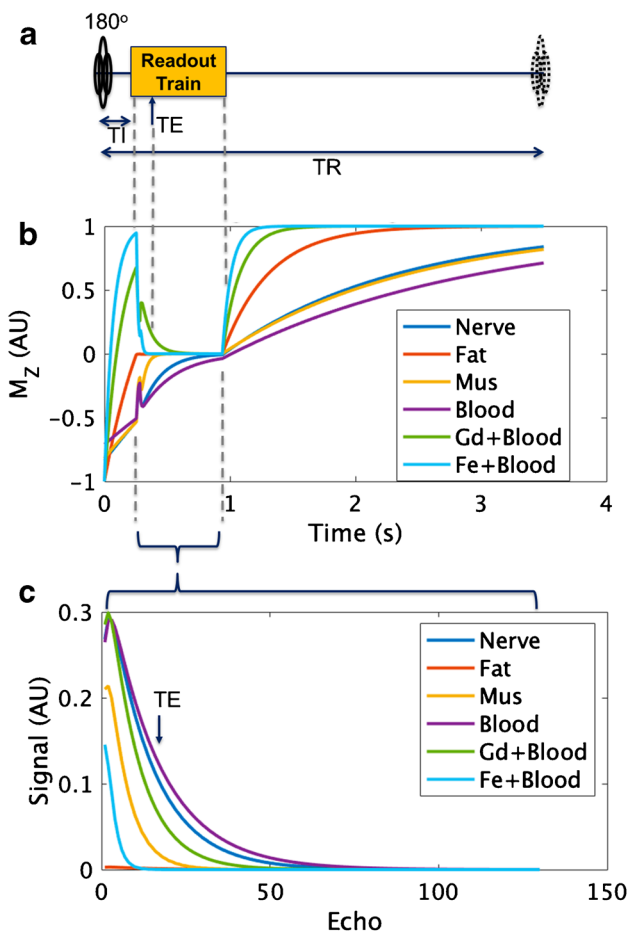


**Fig. 2** (a) Pulse sequence diagram of STIR-FSE, showing inversion time (TI), echo time (TE), and repetition time (TR) relative to the inversion ( $180^\circ$ ) pulse and FSE readout train; (b) longitudinal magnetization ( $M_z$ ) for various simulated tissue species; (c) resulting simulated signal for the readout train, with the position of TE indicated

improved vascular suppression at both low and high velocities. Ferumoxytol was more effective than gadolinium. The extent of vascular suppression within slow-flowing vessels at even a low concentration of ferumoxytol (CR ~20–25 at 25–30% concentration) was similar to the suppression achieved in fast-flowing vessels with no contrast agent administered.

## Human subjects

Twelve subjects were identified and screened for inclusion; one was excluded due to the presence of a large lipoma displacing the brachial plexus and another for low signal-to-noise ratio due to improper coil positioning. In total, 10 subjects were included in the analysis (all female, mean age:

41 years, range 20–51 years). Nine subjects completed bilateral plexus MRIs, giving a total of 19 pre- and post-infusion imaging data sets (10 left, 9 right). The average body mass index was  $30.6 \text{ kg/m}^2$  (range  $19.7\text{--}40.8 \text{ kg/m}^2$ ). Total blood volume, calculated from Nadler's equation, averaged 4.6 L (range  $3.2\text{--}5.6 \text{ L}$ ) [34]. Subjects received, on average, 6 mg ferumoxytol/kg body mass (range  $4.5\text{--}10 \text{ mg/kg}$ ). Five subjects had received ferumoxytol infusions previously, at an average of 17.5 weeks (range 4–31 weeks) prior to study enrollment.

Pre-infusion MR neurography exams were performed, on average, 10 h prior to infusion (range 1–56 h). Post-infusion exams were performed, on average, 70 min following infusion (range 1–2 h). As ferumoxytol has a blood-pool half-life of 14 h when administered as a standard infusion, the  $\leq 2\text{-h}$  delay between infusion and imaging was well within the window of ferumoxytol's blood-pool effect. No adverse events occurred.

## Quantitative analysis

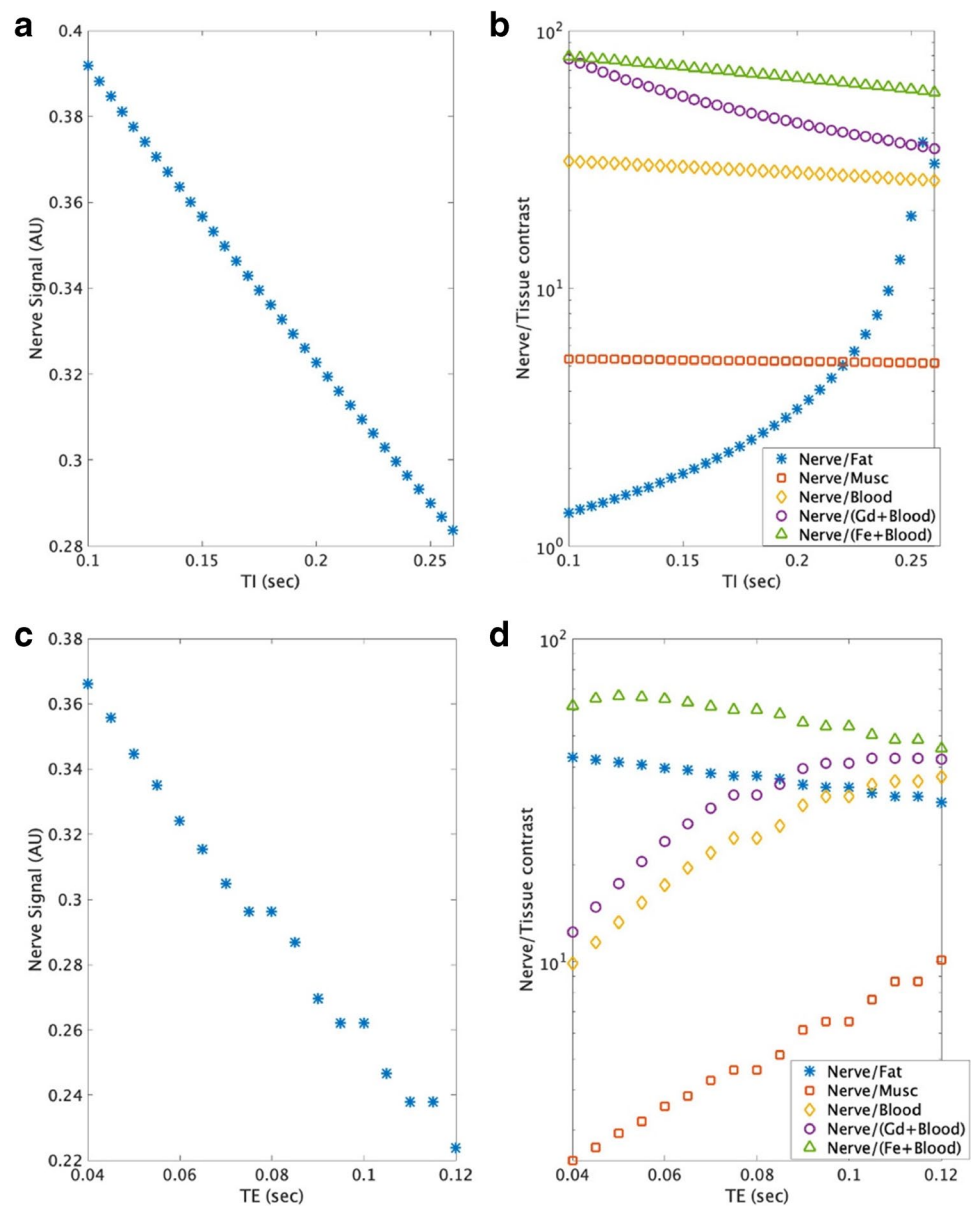
While ferumoxytol did not increase the nerve/fat CR (Fig. 5, CR difference = post minus pre = +1.43, 95% CI:  $-1.89$  to  $4.75$ ,  $p=0.381$ ), the nerve/muscle CR was significantly increased (CR difference = +0.76, 95% CI:  $0.35$  to  $1.18$ ,  $p=0.001$ ). Also, while nerve/large vessel CR was not increased with ferumoxytol (difference = +4.03, 95% CI:  $-0.85$  to  $8.91$ ,  $p=0.102$ ), nerve/small vessel CR was significantly increased (difference = +4.66, 95% CI:  $0.88$  to  $8.43$ ,  $p=0.018$ ).

## Qualitative analysis

Overall vascular suppression improved following ferumoxytol administration, with complete suppression in 90–95% of post-ferumoxytol exams (rater 1:  $\Delta = +1$ ,  $p=0.002$ ; rater 2:  $\Delta = +2$ ,  $p<0.003$ ;  $\Delta$  = median post-pre score difference based on a 3-point scale) (Table 3).

Nerve visualization and diagnostic confidence scores are displayed in Table 3. Visualization and diagnostic confidence were significantly improved by ferumoxytol for both proximal and distal segments of the suprascapular nerve (Table 3, Fig. 6). Diagnostic confidence was improved in rater 1 for the proximal segment of the long thoracic nerve (Fig. 7). All other nerve visualization and diagnostic confidence comparisons were not statistically significant. Visualization and diagnostic confidence of the axillary nerve were “full” (visualization) and “high” (confidence) in the vast majority of both pre- and post-ferumoxytol exams (proximal: 90–100%, distal: 83–100%). However, visualization and diagnostic confidence of the long thoracic nerve were mostly “none” (visualization) and “low” (confidence), including on post-ferumoxytol exams (proximal: 38–100%, distal: 53–100%).

**Fig. 3** Simulated tissue signals with varying (a–b) inversion time (TI), showing optimum fat suppression (high nerve/fat contrast ratio (CR)) at TI~250–255 ms. Simulated tissues with varying (c–d) echo time (TE) show decreased nerve signal with increased TE but increased nerve/muscle CR with increased TE. Nerve/(Fe+ blood) and nerve/fat CRs were fairly constant with TE



The inter-rater agreement for vascular suppression (Table 4) was higher in post-ferumoxytol exams (substantial for pre- and near-perfect for post-ferumoxytol exams). Inter-rater agreement for visualization and diagnostic confidence in the suprascapular and axillary nerve segments was higher in post- than in pre-ferumoxytol exams. The converse was true for the long thoracic nerve segments.

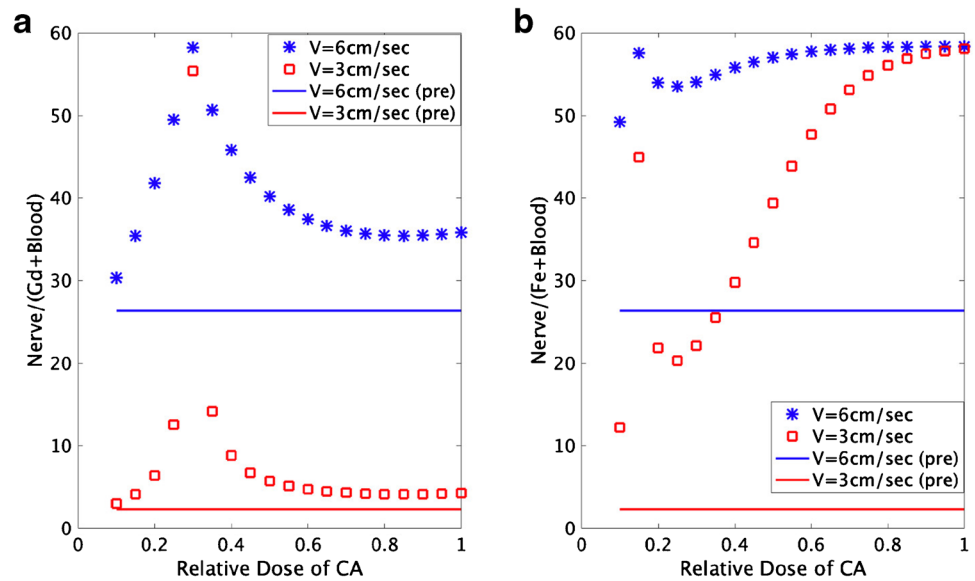
## Discussion

In this study, ferumoxytol was shown to provide robust vascular suppression in MR neurography in healthy subjects without neuropathy, improving both qualitative assessments (vascular suppression, nerve visualization, and diagnostic

confidence) and quantitative nerve/muscle and nerve/small vessel contrast. The quantitative, in vivo findings were mostly anticipated by the simulations. The unexpected improvement in nerve-to-muscle signal contrast, however, was likely due to contribution from muscle microvasculature, which was not simulated. Additionally, simulation CRs were mostly higher than in vivo CRs. This was likely due to higher image noise in vivo and patient bulk motion that was also not simulated.

Ferumoxytol significantly improved visualization and diagnostic confidence in assessing the suprascapular nerve and less so in the axillary and long thoracic nerves. As the axillary nerve was already well seen in pre-ferumoxytol exams, the relative improvement with ferumoxytol was not as clinically important. Conversely, the long thoracic nerve remains challenging to

**Fig. 4** Simulated nerve/blood contrast ratios (CRs) with different doses of Gd contrast agents (CA), showing (a) optimum nerve/(Gd + blood) ratio at a relative dose of ~0.3, higher ratios at higher blood velocities (V). Simulated CRs for (b) Fe CA show higher nerve/(Fe + blood) CRs than Gd and fairly constant and high nerve/(Fe + blood) CRs at V = 6 cm/s. Nerve/(Fe + blood) CR are lower at V = 3 cm/s but peak at a relative dose of ~0.15



visualize in MR neurography, even with ferumoxytol-enhanced vascular suppression. This is likely due to the nerve’s small size, tortuous course, and proximity to the chest wall, which results in obscuration from respiratory motion artifact. Additionally, coils used for plexus imaging are centered over the neck/shoulder regions and may provide insufficient coverage along the chest wall in larger patients. While direct statistical comparison of differences in qualitative grades between the two raters was not performed, the less experienced rater (rater 2) did notice an overall greater improvement in nerve visualization in the presence of ferumoxytol for both the suprascapular and axillary nerve proximal and distal segments as well as greater improvement in diagnostic confidence for the suprascapular nerve distal segment (Table 3).

Gadolinium-based contrast agents have been previously used to achieve vascular suppression in MR neurography of the brachial plexus [12–14]. Comparing results from the present pilot study against a previous work by our group with a similar methodology [14], ferumoxytol seems to provide similar or superior nerve conspicuity and diagnostic confidence relative to gadolinium. Although ferumoxytol was not directly compared against gadolinium in vivo, its superior vascular suppression is supported by the simulation results. Crusher gradients, which lengthen the echo spacing causing blurring, were additionally used in combination with intravenous ferumoxytol in the present study to achieve vascular suppression. Based on our anecdotal experience and simulations, crusher gradients may not be

**Fig. 5** Nerve/tissue contrast ratios (CRs) for pre- and post-ferumoxytol scans. Statistically significant (paired *t*-test,  $p < 0.05$ ) indicated by an asterisk (\*)

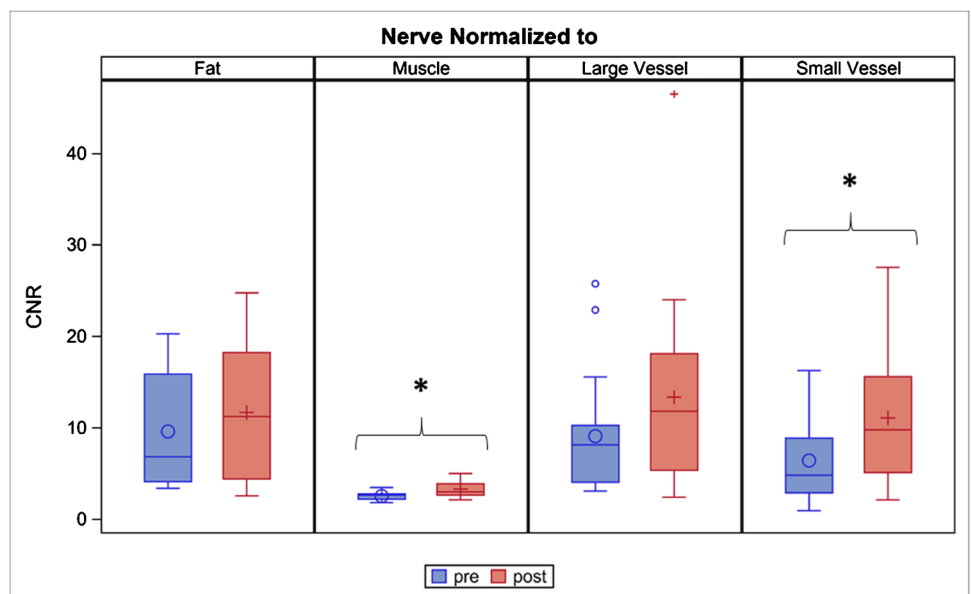


**Table 3** Vascular suppression, nerve visualization, and diagnostic confidence scores for each rater

Metric		Pre		Post		Post vs. Pre			
		Rater 1	Rater 2	Rater 1	Rater 2	Rater 1		Rater 2	
		<i>n</i> (%)	<i>n</i> (%)	<i>n</i> (%)	<i>n</i> (%)	$\Delta$	<i>p</i> -value	$\Delta$	<i>p</i> -value
Vascular suppression	1	0 (0)	12 (63.2)	0 (0)	0 (0)	1 [1, 1]	0.002	2 [1, 2]	0.003
	2	19 (100)	7 (36.8)	2 (10.5)	1 (5.3)				
	3	0 (0)	0 (0)	17 (89.5)	18 (94.7)				
Nerve visualization*									
Proximal suprascapular N	None	1 (5.3)	1 (5.3)	0 (0)	0 (0)	0 [0, 1]	0.045	0 [0, 1]	0.014
	Partial	6 (31.6)	11 (57.9)	1 (5.9)	3 (17.6)				
	Full	12 (63.2)	7 (36.8)	16 (94.1)	14 (82.4)				
Distal suprascapular N	None	1 (5.3)	0 (0)	0 (0)	0 (0)	1 [0, 1]	0.015	1 [1, 1]	0.003
	Partial	9 (47.4)	15 (78.9)	0 (0)	0 (0)				
	Full	9 (47.4)	4 (21.1)	19 (100)	19 (100)				
Proximal axillary N	None	0 (0)	0 (0)	0 (0)	0 (0)	0 [0, 0]	0.999	0 [0, 0]	0.500
	Partial	1 (5.3)	2 (10.5)	0 (0)	0 (0)				
	Full	18 (94.7)	17 (89.5)	19 (100)	19 (100)				
Distal axillary N	None	0 (0)	0 (0)	0 (0)	0 (0)	0 [0, 0]	0.999	0 [0, 0]	0.250
	Partial	1 (5.6)	3 (16.7)	0 (0)	0 (0)				
	Full	17 (94.4)	15 (83.3)	19 (100)	19 (100)				
Proximal long thoracic N	None	7 (36.8)	19 (100)	6 (37.5)	16 (100)	0 [0, 1]	0.213	0 [0, 0]	-
	Partial	11 (57.9)	0 (0)	4 (25)	0 (0)				
	Full	1 (5.3)	0 (0)	6 (37.5)	0 (0)				
Distal long thoracic N	None	16 (84.2)	16 (84.2)	10 (52.6)	14 (73.7)	0 [0, 1]	0.067	0 [0, 1]	0.325
	Partial	2 (10.5)	3 (15.8)	6 (31.6)	3 (15.8)				
	Full	1 (5.3)	0 (0)	3 (15.8)	2 (10.5)				
Diagnostic confidence*									
Proximal suprascapular N	Low	10 (52.6)	11 (57.9)	1 (5.9)	1 (5.9)	1 [0, 1]	0.016	1 [0, 1]	0.014
	High	9 (47.4)	8 (42.1)	16 (94.1)	16 (94.1)				
Distal suprascapular N	Low	9 (47.4)	13 (68.4)	0 (0)	0 (0)	0 [0, 1]	0.023	1 [0, 1]	0.007
	High	10 (52.6)	6 (31.6)	19 (100)	19 (100)				
Proximal axillary N	Low	2 (10.5)	1 (5.3)	0 (0)	0 (0)	0 [0, 0]	0.500	0 [0, 0]	0.999
	High	17 (89.5)	18 (94.7)	19 (100)	19 (100)				
Distal axillary N	Low	3 (16.7)	3 (16.7)	0 (0)	0 (0)	0 [0, 0]	0.250	0 [0, 0]	0.250
	High	15 (83.3)	15 (83.3)	19 (100)	19 (100)				
Proximal long thoracic N	Low	18 (94.7)	19 (100)	10 (62.5)	16 (100)	0 [0, 1]	0.048	0 [0, 0]	-
	High	1 (5.3)	0 (0)	6 (37.5)	0 (0)				
Distal long thoracic N	Low	19 (0)	19 (0)	17 (89.5)	18 (94.7)	0 [0, 0]	0.500	0 [0, 0]	0.999
	High	0 (0)	0 (0)	2 (10.5)	1 (5.3)				

\*  $n < 19$  in categories where the nerve segment could not be graded because it was out of the imaged field of view (distal axillary [1], proximal long thoracic [2]) or due to poor signal-to-noise ratio (SNR) (proximal suprascapular [2], proximal long thoracic [1])

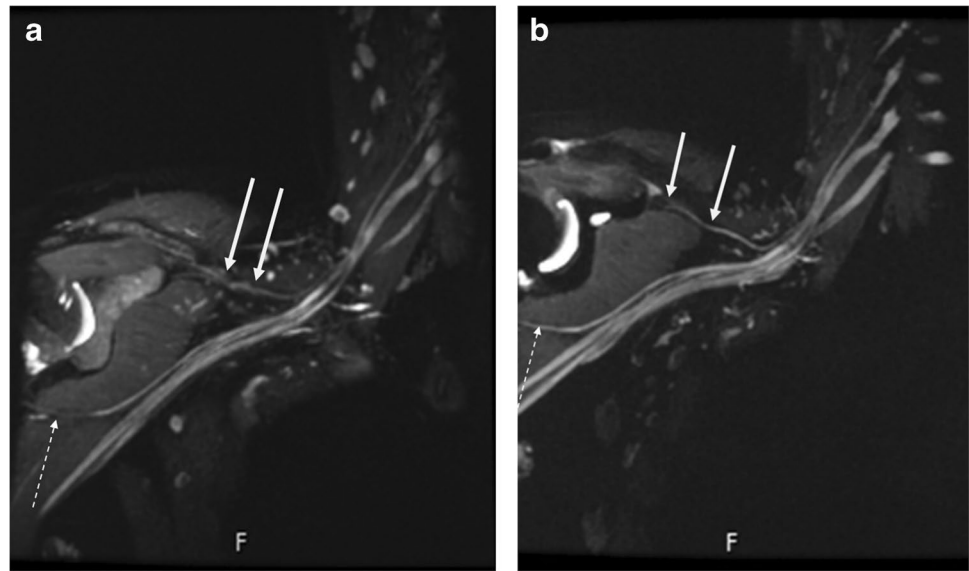
needed given ferumoxytol's high  $r_2^*$ ; in contrast, crusher gradients are likely needed with gadolinium to achieve full vascular suppression. Simulation results suggest that the imaging parameters (TI, TE) for non-contrast STIR-FSE are appropriate for either gadolinium- or ferumoxytol-enhanced imaging. Similar imaging parameters will facilitate the comparison of pre- and post-contrast imaging for research and clinical purposes, particularly in cases where vasculature impedes diagnosis in pre-contrast scans. As

only subjects without known peripheral neuropathies were recruited in this pilot study, additional studies that directly assess ferumoxytol's efficacy in patients with neuropathies are needed to validate its clinical utility.

We acknowledge several study limitations, including the small number of study participants. Another possible limitation is that velocities were not measured in the "small" vessel chosen for contrast analysis (i.e. the suprascapular artery); as such, simulated velocities were estimated and not



**Fig. 6** 20-year-old female with normal brachial plexus. Pre-ferumoxytol 3D STIR-FSE multiplanar reformatted (MPR) maximal intensity projection (MIP) (a) demonstrates venous contamination obscuring the distal segment of the suprascapular nerve (solid arrows) and poor delineation of the distal segment of the axillary nerve (thin, dashed arrow) due to relatively poor nerve-to-muscle contrast. On the post-ferumoxytol MPR MIP, the suprascapular and axillary nerves are clearly delineated



matched to in vivo results. A vein was not chosen, as veins were difficult to reliably visualize on post-ferumoxytol exams as a result of effective vascular suppression. Additionally, while attempts to standardize imaging conditions were made, slight variations in the obliquity of the imaging field of view, patient anatomy due to positioning, and variable coil positioning around different body habitus were unavoidable.

Since the U.S. Food and Drug Administration (FDA) approved ferumoxytol in 2009 to treat iron deficiency anemia, over 2.6 million therapeutic doses have been administered [35]. Ferumoxytol is currently prescribed therapeutically as a standard, slow infusion of 510 mg elemental iron in 200 mL normal saline over 15 min [35]. When infused slowly, ferumoxytol has an excellent safety record. This contrasts with early reports of

anaphylaxis or anaphylactoid reactions associated with a rapid, 17-s bolus injection [36]. A recent systematic review and meta-analysis of 39 studies evaluating ferumoxytol for off-label imaging applications, including 5411 ferumoxytol administrations in 4336 patients, found an overall adverse event rate of 2%. Of these events, 99% were minor or moderate in severity and no deaths were reported [16]. There was a single report of suspected anaphylaxis in a patient who developed hypotension and was treated with vasopressors and intubation [37]. In another meta-analysis evaluating 4240 off-label diagnostic ferumoxytol infusions in 3215 patients across 11 different sites, no ferumoxytol-related severe or life-threatening adverse events occurred [38].

Off-label, clinical imaging applications of ferumoxytol have previously taken advantage of its unique

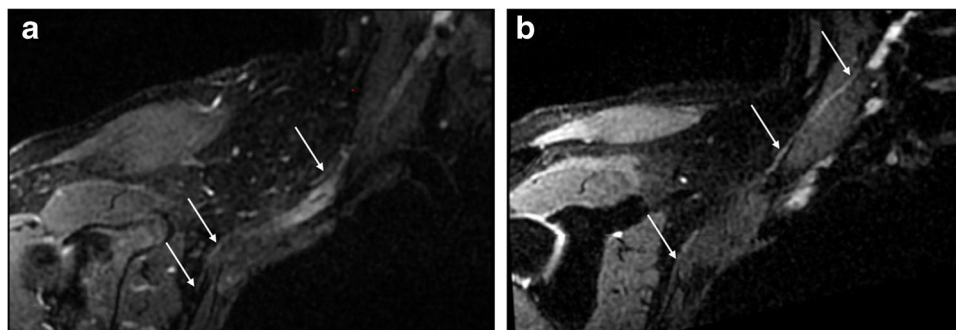


**Fig. 7** 50-year-old female with normal brachial plexus. Pre-ferumoxytol 3D STIR-FSE curved multiplanar reformatted (MPR) (a) demonstrates venous contamination and relatively low nerve-to-muscle contrast enabling only a very short segment of the long thoracic

nerve (arrows) to be visualized. On the post-ferumoxytol curved MPR (b), a much longer segment of the long thoracic nerve (arrows), inclusive of its proximal C6 nerve root contribution, is delineated

**Table 4** Inter-rater agreement between pre-ferumoxytol and post-ferumoxytol exams for overall vascular suppression, nerve visualization, and diagnostic confidence

Metric		Pre AC2 (SE)*	Post AC2 (SE)*
Vascular suppression	Proximal suprascapular nerve	0.64 (0.09)	0.94 (0.04)
	Distal suprascapular nerve	0.75 (0.09)	0.95 (0.04)
	Proximal axillary nerve	0.74 (0.08)	1.00 (0.00)
	Distal axillary nerve	0.57 (0.13)	0.17 (0.28)
	Proximal long thoracic nerve	0.81 (0.10)	0.65 (0.14)
	Distal long thoracic nerve	0.94 (0.04)	1.00 (0.00)
Diagnostic confidence	Proximal suprascapular nerve	0.95 (0.03)	1.00 (0.00)
	Distal suprascapular nerve	0.69 (0.17)	0.87 (0.10)
	Proximal axillary nerve	0.59 (0.19)	1.00 (0.00)
	Distal axillary nerve	0.94 (0.06)	0.46 (0.24)
	Proximal long thoracic nerve	1.00 (0.00)	0.82 (0.12)
	Distal long thoracic nerve	0.94 (0.06)	1.00 (0.00)
	Distal long thoracic nerve	0.85 (0.12)	1.00 (0.00)

\*AC2, agreement coefficient 2 for weighted analysis, ordinal scale grades; SE, standard error

Strength of agreement: <0=poor; 0.00–0.2=slight; 0.21–0.40=fair agreement; 0.41–0.60=moderate; 0.61–0.80=substantial; 0.81–1=almost perfect

properties, including the “black blood” appearance of vessels on T<sub>2</sub>-weighted sequences (for MR angiography, MR lymphangiography, vessel wall, and cardiac imaging), its long intravascular half-life of 10–14 h (steady-state imaging, evaluating the extent of tumor resection intra- and post-op without repeat gadolinium) and phagocytic elimination from the bloodstream (tumors, vessel wall inflammation) [11, 22–25]. These properties of ferumoxytol confer similar advantages in MR neurography; in addition to vascular suppression, the steady intravascular concentration of ferumoxytol allows scans to be repeated due to respiratory or motion artifact and for imaging of multiple stations to evaluate distal peripheral nerve territories.

Limitations of incorporating ferumoxytol into clinical practice include its higher cost compared to most gadolinium-based contrast agents, slower workflow due to its slow infusion, and the need for monitoring patient vital signs (up to 30 min post-infusion). The inherent and potential diagnostic advantages of ferumoxytol, however, may offset these limitations, especially if doses are reduced. A potential clinical limitation of ferumoxytol is its impact on MRI interpretation due to altered signal intensities for days to months following administration. Although the FDA label cautions that ferumoxytol can affect T<sub>2</sub>-weighted MRI for up to 3 months, some published reviews have mentioned this interval could be days, weeks, or months [20, 38]. It is also conceivable that a lower dose of ferumoxytol would further reduce this interval.

Overall, this study showed that ferumoxytol can be used to achieve effective vascular suppression in MR

neurography of the brachial plexus. Importantly, the simulations suggest that ferumoxytol can be infused at significantly lower doses (~15–30% of a single therapeutic dose) to achieve effective vascular suppression. Incidentally, the simulations also suggest that a lower dose (~30%) of gadolinium injections may provide effective vascular suppression. With a slow infusion and reduced dosage, ferumoxytol may offer a more favorable safety profile than gadolinium-based contrast agents, particularly in patients with chronic kidney disease and given concerns over uncertain effects from long-term gadolinium deposition in the brain, spinal cord, and peripheral nerves [15, 17, 19, 39]. Future research studies should evaluate the use of ferumoxytol to visualize other clinically important nerves, as well the diagnostic utility of this technique in patients with suspected peripheral neuropathies.

**Abbreviations** CR, Contrast ratio; IDA, Iron deficiency anemia; TE, Echo time; TI, Inversion time; TR, Repetition time

**Acknowledgements** The authors would like to thank Drs. John Carrino and Steven P. Daniels for their motivation for the project and support.

Hospital for Special Surgery has an institutional research agreement with General Electric Healthcare.

**Funding** This study was funded by a Seed Grant from the International Skeletal Society (ISS).

## Declarations

**Ethical approval** All procedures performed in studies involving human participants were in accordance with the ethical standards of the insti-

tutional and/or national research committee and with the 1964 Helsinki declaration and its later amendments or comparable ethical standards.

**Disclaimer** Its contents are solely the responsibility of the authors and do not necessarily represent the official views of the ISS.

## References

- Filler A. Magnetic resonance neurography and diffusion tensor imaging: origins, history, and clinical impact of the first 50,000 cases with an assessment of efficacy and utility in a prospective 5000-patient study group. *Neurosurgery*. 2009;65(4 Suppl):A29–43.
- Does MD, Snyder RE. T2 relaxation of peripheral nerve measured in vivo. *Magn Reson Imaging*. 1995;13(4):575–80.
- Yoneyama M, Takahara T, Kwee TC, et al. Rapid high resolution MR neurography with a diffusion-weighted pre-pulse. *Magn Reson Med Sci*. 2013;12:111–9.
- Cervantes B, Kirschke JS, Klupp E, et al. Orthogonally combined motion- and diffusion-sensitized driven equilibrium (OC-MDSDE) preparation for vessel signal suppression in 3D turbo spin echo imaging of peripheral nerves in the extremities. *Magn Reson Med*. 2018;79:407–15.
- Chhabra A, Subhawong TK, Bizzell C, et al. 3T MR neurography using three dimensional diffusion-weighted PSIF: technical issues and advantages. *Skeletal Radiol*. 2011;40:1355–60.
- Xu X et al. Investigation of 3D reduced field of view carotid atherosclerotic plaque imaging. *Magn Reson Imaging*. 2017.
- Lindenholz A, et al. The use and pitfalls of intracranial vessel wall imaging: how we do it. *Radiology*. 2017;286(1):12–28.
- Abdel-Aty H, Simonetti O, Friedrich MG. T2-weighted cardiovascular magnetic resonance imaging. *J Magn Reson Imaging*. 2007;26(3):452–9.
- Brown R, et al. Effect of blood flow on double inversion recovery vessel wall MRI of the peripheral arteries: quantitation with T2 mapping and comparison with flow-insensitive T2-prepared inversion recovery imaging. *Magnetic resonance in medicine : official journal of the Society of Magnetic Resonance in Medicine / Society of Magnetic Resonance in Medicine*. 2010;63(3):736–44.
- Deshmukh S, Fayad LM, Ahlawat S. MR neurography (MRN) of the long thoracic nerve: retrospective review of clinical findings and imaging results at our institution over 4 years. *Skeletal Radiol*. 2017;46(11):1531–40.
- Aime S, Caravan P. Biodistribution of gadolinium-based contrast agents, including gadolinium deposition. *J Magn Reson Imaging*. 2009;30:1259–67.
- Chen WC, Tsai YH, Weng HH, et al. Value of enhancement technique in 3D–T2 STIR images of the brachial plexus. *J Comput Assist Tomogr*. 2014;38:335–9.
- Wang L, Niu Y, Kong X, et al. The application of paramagnetic contrast-based T2 effect to 3D heavily T2W high-resolution MR imaging of the brachial plexus and its branches. *Eur J Radiol*. 2016;85:578–84.
- Sneag DB, Daniels SP, Geannette C, et al. Post-contrast 3D inversion recovery magnetic resonance neurography for evaluation of branch nerves of the brachial plexus. *Eur J Radiol*. 2020;28(132):109304.
- Kanda T, Ishii K, Kawaguchi H, Kitajima K, Takenaka D. High signal intensity in the dentate nucleus and globus pallidus on unenhanced T1-weighted MR images: relationship with increasing cumulative dose of a gadolinium-based contrast material. *Radiology*. 2014;270(3):834–41.
- Ahmad F, Treanor L, McGrath TA, Walker D, McInnes MDF, Schieda N. Safety of off-label use of ferumoxytol as a contrast agent for MRI: a systematic review and meta-analysis of adverse events. *J Magn Reson Imaging*. 2021;53(3):840–58.
- Alkhunizi SM, Fakhoury M, Abou-Kheir W, Lawand N. Gadolinium retention in the central and peripheral nervous system: implications for pain, cognition, and neurogenesis. *Radiology*. 2020;297(2):407–16.
- Grobner T. Gadolinium—a specific trigger for the development of nephrogenic fibrosing dermopathy and nephrogenic systemic fibrosis? *Nephrol Dial Transplant*. 2006;21(4):1104–8.
- McDonald JS, McDonald RJ. MR imaging safety considerations of gadolinium-based contrast agents: gadolinium retention and nephrogenic systemic fibrosis. *Magn Reson Imaging Clin N Am*. 2020;28(4):497–507.
- Toth GB, Varallyay CG, Horvath A, et al. Current and potential imaging applications of ferumoxytol for magnetic resonance imaging. *Kidney Int*. 2017;92(1):47–66.
- Daldrup-Link HE. Ten things you might not know about iron oxide nanoparticles. *Radiology*. 2017;284(3):616–29.
- Knobloch G, Colgan T, Wiens C, et al. Relaxivity of ferumoxytol at 1.5 T and 3.0 T. *Invest Radiol*. 2018;53(5):257–63.
- Nguyen KL, Park EA, Yoshida T, Hu P, Finn JP. Ferumoxytol enhanced black-blood cardiovascular magnetic resonance imaging. *J Cardiovasc Magn Reson*. 2017;19(1):106.
- Wu W, Klockow JL, Mohanty S, Ku KS, Aghighi M, Mellemenidis S, et al. Theranostic nanoparticles enhance the response of glioblastomas to radiation. *Nanotheranostics*. 2019;3(4):299–310.
- Prince MR, Zhang HL, Chabra SG, Jacobs P, Wang Y. A pilot investigation of new superparamagnetic iron oxide (ferumoxytol) as a contrast agent for cardiovascular MRI. *J Xray Sci Technol*. 2003;11(4):231–40.
- Stirrat CG, et al. Ferumoxytol-enhanced magnetic resonance imaging methodology and normal values at 1.5 and 3T. *J Cardiovasc Magn Reson*. 2016;18(1):1–9.
- Maki JH, et al. Dark blood magnetic resonance lymphangiography using dual-agent relaxivity contrast (DARC-MRL): a novel method combining gadolinium and iron contrast agents. *Curr Probl Diagn Radiol*. 2016;45(3):174–9.
- Mitsumori LM, et al. Peripheral magnetic resonance lymphangiography: techniques and applications. *Tech Vasc Interv Radiol*. 2016;19(4):262–72.
- Datta S, Satten G. A signed-rank test for clustered data. *Biometrics*. 2008;64:501–7.
- Durkalski V, Palesch Y, Lipsitz S, Rust P. Analysis of clustered matched pair data. *Stat Med*. 2003;22:2417–28.
- Gregg M. Marginal methods and software for clustered data with cluster- and group-size informativeness. PhD dissertation, University of Louisville, 2020.
- Gwet KL. Computing inter-rater reliability and its variance in the presence of high agreement. *Br J Math Stat Psychol*. 2008;61:29–48.
- Gregg M, Datta S, Lorenz D. htestClust: reweighted marginal hypothesis tests for clustered data. R package version 0.2.0. <https://CRAN.R-project.org/package=hstestClust>. 2020.
- Nadler SBB, Hidalgo JHH, Bloch T. Prediction of blood volume in normal human adults. *Surgery*. 1962;51:224–32.
- Data on file. AMAG Pharmaceuticals, Inc. <https://www.feraheme.com/>. Accessed 4 May 2021.
- US Food and Drug Administration. FDA drug safety communication: FDA strengthens warnings and changes prescribing instructions to decrease the risk of serious allergic reactions with anemia drug Feraheme (ferumoxytol). Accessed on March

- 19, 2021. Available from: <http://www.fda.gov/Drugs/DrugSafety/ucm440138.htm>.
37. Wise-Faberowski L, Velasquez N, Chan F, Vasanawala S, McElhinney DB, Ramamoorthy C. Safety of ferumoxytol in children undergoing cardiac MRI under general anaesthesia. *Cardiol Young*. 2018;28(7):916–21.
38. Nguyen KL, Yoshida T, Kathuria-Prakash N, et al. Multicenter safety and practice for off-label diagnostic use of ferumoxytol in MRI. *Radiology*. 2019;293(3):554–64.
39. Neuwelt EA, Hamilton BE, Varallyay CG, et al. Ultrasmall superparamagnetic iron oxides (USPIOs): a future alternative magnetic resonance (MR) contrast agent for patients at risk for nephrogenic systemic fibrosis (NSF)? *Kidney Int*. 2009;75(5):465–74.

**Publisher's note** Springer Nature remains neutral with regard to jurisdictional claims in published maps and institutional affiliations.